JOURNAL OF VIROLOGY, Jan. 2009, p. 408–419 Vol. 83, No. 1
0022-538X/09/$08.00+0 doi:10.1128/JVI.01568-08

Exploring the Nuclear Envelope of Herpes Simplex Virus 1-Infected Cells by High-Resolution Microscopy▽

Peter Wild,[1]* Claudia Senn,[2] Céline L. Manera,[1] Esther Sutter,[1] Elisabeth M. Schraner,[1] Kurt Tobler,[2] Mathias Ackermann,[2] Urs Ziegler,[3] Miriam S. Lucas,[4] and Andres Kaech[4]†

Electron Microscopy, Institute of Veterinary Anatomy,[1] Institute of Virology,[2] and Center for Microscopy and Image Analysis,[3] University of Zürich, and Electron Microscopy ETH Zürich, Swiss Federal Institute of Technology,[4] Zürich, Switzerland

Received 24 July 2008/Accepted 6 October 2008

Herpesviruses are composed of capsid, tegument, and envelope. Capsids assemble in the nucleus and exit the nucleus by budding at the inner nuclear membrane, acquiring tegument and the envelope. This study focuses on the changes of the nuclear envelope during herpes simplex virus 1 (HSV-1) infection in HeLa and Vero cells by employing preparation techniques at ambient and low temperatures for high-resolution scanning and transmission electron microscopy and confocal laser scanning microscopy. Cryo-field emission scanning electron microscopy of freeze-fractured cells showed for the first time budding of capsids at the nuclear envelope at the third dimension with high activity at 10 h and low activity at 15 h of incubation. The mean number of pores was significantly lower, and the mean interpore distance and the mean interpore area were significantly larger than those for mock-infected cells 15 h after inoculation. Forty-five percent of nuclear pores in HSV-1-infected cells were dilated to more than 140 nm. Nuclear material containing capsids protrude through them into the cytoplasm. Examination of in situ preparations after dry fracturing revealed significant enlargements of the nuclear pore diameter and of the nuclear pore central channel in HSV-1-infected cells compared to mock-infected cells. The demonstration of nucleoporins by confocal microscopy also revealed fewer pores but focal enhancement of fluorescence signals in HSV-1-infected cells, whereas Western blots showed no loss of nucleoporins from cells. The data suggest that infection with HSV-1 alters the number, size, and architecture of nuclear pores without a loss of nucleoporins from altered nuclear pore complexes.

The nuclear envelope separates eukaryotic cells into a nuclear compartment and a cytoplasmic compartment. It comprises two phospholipid bilayers, the inner and the outer nuclear membrane. Local fusions between both membranes create giant aqueous channels, the nuclear pores, through which nucleocytoplasmic exchanges proceed. Elaborate protein structures of eightfold rotational symmetry, the nuclear pore complexes (NPC), are embedded into these pores (14, 28). Each NPC is composed of building blocks of ~30 different proteins called nucleoporins (Nup). Nucleoporins are modularly assembled to form subcomplexes within the highly dynamic NPC (9, 46).

Herpesvirus virions consist of the genomic double-stranded DNA enclosed by an icosahedral capsid, the tegument proteins, and the viral envelope (44). During infection, newly synthesized capsid proteins are transported from the cytoplasm to the nucleus, where they assemble autocatalytically to capsids into which DNA is packaged. This process resembles head assembly and DNA packaging in bacteriophages (40). Assembled capsids are transported to the nuclear periphery. There, they bud at the inner nuclear membrane, acquiring tegument and the viral envelope. The replication of herpesviruses such as herpes simplex virus 1 (HSV-1) radically alters nuclear architecture (48). In particular, the nuclear membrane becomes highly modified in the course of viral replication (44).

The nuclear periphery of herpesvirus-infected cells has been studied intensely by conventional transmission electron microscopy (TEM) on thin sections (for reviews, see references 31, 32, and 33). Imaging of the nuclear surface by applying other techniques such as scanning electron microscopy (SEM) was rare because the advantages of surface imaging at the subcellular level by SEM were not available to cell biologists due largely to insufficient resolutions of the scanning electron microscopes. This situation was considerably improved by the introduction of field emission sources. They facilitate surface imaging at much the same effective resolution for biological material as that of TEM (2, 23). An alternative methodology for surface imaging is the technique of freeze fracture, which is followed by the production of replicas for imaging by TEM (21). Although this technology is cumbersome to apply to isolated cells, it has been successfully employed to visualize the nuclear surface of HSV-1-infected BHK-21 cells (22).

The introduction of field emission SEM (FESEM) and the development of methodologies to image the surface of subcellular structures in the dried state (1) as well as in the frozen-hydrated state (56) led to detailed information for subcellular structures such as the nuclear surface. Here, we employed cryopreparation techniques for cell suspensions as well as in situ preparation techniques for cell monolayers at ambient temperatures with the aim to obtain a more detailed view of the nuclear surface in HSV-1-infected cells. Imaging of the nuclear surface in the dried state of HSV-1-infected cells revealed a reduction in the number of nuclear pores. It also showed substantial enlargements of the

* Corresponding author. Mailing address: Electron Microscopy, Institute of Virology, Winterthurerstrasse 266a, CH-8057 Zürich, Switzerland. Phone: 41 1 635 87 84. Fax: 41 1 635 89 11. E-mail: pewild@vetanat.uzh.ch.

† Present address: Center for Microscopy and Image Analysis, University of Zürich, Zürich, Switzerland.

▽ Published ahead of print on 15 October 2008.

overall diameter of NPCs as well as of the central NPC channel compared to those of mock-infected cells. Imaging of the nuclear surface in the frozen-hydrated state confirmed the reduction of pore numbers and dilation of nuclear pores through which nuclear material containing capsids protrude into the cytoplasm, as shown by TEM of cells prepared in situ by employing cryofixation and freeze substitution. By employing confocal microscopy for third-dimension reconstruction, the nuclear volume and nuclear surface area were calculated, which in turn allowed the calculation of pore numbers and budding events per total nuclear surface. In addition, cryo-FESEM allowed for the first time the visualization of budding capsids at the third dimension, revealing the greatest budding activity as early as 10 h after infection.

MATERIALS AND METHODS

Viruses and cells. Vero and HeLa cells were grown in Dulbecco's modified minimal essential medium supplemented with penicillin (100 U/ml), streptomycin (100 g/ml), and 10% fetal bovine serum for 2 days. The cells were then infected with HSV-1 at a multiplicity of infection (MOI) of 2 or 5 and incubated at 37°C for 8 to 24 h.

FESEM. In order to examine the nuclear surface, a protocol for in situ preparation of nuclei according to that described previously by Allen et al. (3) was applied. Cells were grown on glass coverslips for 2 days and then infected with HSV-1 at an MOI of 5 and incubated at 37°C for up to 15 h. The cells were then fixed with 1% formaldehyde plus 0.025% glutaraldehyde in 0.1 M Na/K-phosphate (pH 7.4) at room temperature for 1 min and permeabilized with 0.5% Triton X-100 for 5 min. After postfixation with 1% osmium tetroxide at 4°C for 30 min, cells were treated with 1% aqueous thiocarbohydrazide at room temperature for 30 min. After additional fixation with 1% osmium tetroxide at room temperature for 30 min, cells were dehydrated with a graded series of ethanol starting at 70% and critical point dried (CPD 030; Bal-Tec, Balzers, Liechtenstein). The dry samples were fractured in this way. The glass coverslip with the dry cells on it was laid on an adhesive film on an SEM sample holder. This was firmly touched with another adhesive sample holder and pulled away without sideways movement. The surface on which the cells were grown and the adhesive surface were coated with 5 nm of platinum by sputter coating in a high-vacuum sputtering device (SCD500; Bal-Tec, Balzers, Liechtenstein). The coated samples were examined with a field emission scanning electron microscope (Leo Gemini 1530; Zeiss, Oberkochen, Germany) at an acceleration voltage of 3 kV using the in-lens secondary electron detector.

Cryo-FESEM. HSV-1-infected (MOI of 5) and mock-infected cells grown in cell culture flasks were trypsinized and centrifuged at 150 × *g* for 8 min. The pellet was resuspended in fresh medium, collected into Eppendorf tubes, and fixed with 0.25% glutaraldehyde medium for 30 min. The suspension was kept in the tubes at 4°C until cells were sedimented. Subsequently, the supernatant was removed. A copper grid (100 mesh/inch, 12-μm thickness) was dipped into the sedimented cells, sandwiched between two flat aluminum specimen carriers (type B; Bal-Tec, Balzers, Liechtenstein), and immediately frozen in an HPM 010 high-pressure freezing machine (Bal-Tec). After freezing, the sandwich was mounted under liquid nitrogen on a designated specimen holder for freeze fracturing in the VCT 100 cryopreparation box and transferred onto a BAF 060 freeze-fracturing device (Bal-Tec) using the VCT 100 cryotransfer system (Bal-Tec). The specimen was fractured at −120°C by removing the top aluminum specimen carrier with the hard metal knife supplied with the BAF 060 device. The fractured surfaces were partially freeze-dried ("etched") at −105°C for 2 min in a vacuum of about 10^{-7} mbar. The specimen surface was then coated with 2 nm platinum/carbon by electron beam evaporation at an angle of 45° and with 1 nm platinum/carbon, tilting the electron beam gun between 0° and 90°. The specimen was retracted into the transfer shuttle of the VCT 100 system and transferred under high vacuum onto the cryostage in the SEM (Leo Gemini 1530; Zeiss, Oberkochen, Germany). Specimens were imaged at −115°C (the saturation water vapor pressure of the specimen corresponding to the vacuum in the chamber of 5×10^{-7} mbar) and at an acceleration voltage of 5 kV using the in-lens secondary electron detector.

CFTEM. Cells grown on sapphire disks, infected with HSV-1 (MOI of 5), and incubated at 37°C for 8 to 17 h were fixed with 0.25% glutaraldehyde and then frozen in a high-pressure freezing machine (HPM 010; Bal-Tec) as described previously by Monaghan et al. (34). Frozen cells were transferred into a freeze-substitution unit (FS 7500; Boeckeler Instruments, Tucson, AZ) precooled to −88°C for substitution with acetone and subsequent fixation with 0.25% glutaraldehyde and 0.5% osmium tetroxide at temperatures between −30°C and +2°C as described in detail previously (60) and embedded in Epon. Sections (50 to 60 nm thick) were stained with uranyl acetate and lead citrate and analyzed using a transmission electron microscope (CM12; Philips, Eindhoven, The Netherlands) equipped with a charge-coupled-device camera (Ultrascan 1000; Gatan, Pleasanton, CA) at an acceleration voltage of 100 kV.

Confocal microscopy. Cells were grown for 2 days on 10-mm-diameter coverslips (Mattek, Ashland, MA). The cells were then infected with HSV-1 at an MOI of 5 and incubated at 37°C for 8, 10, 12, 15, and 17 h. After fixation with 2% formaldehyde for 25 min at room temperature, the cells were permeabilized with 0.1% Triton X-100 at room temperature for 7 min and blocked with 3% bovine serum albumin in phosphate-buffered saline containing 0.05% Tween (PBST). To identify nuclear pores, immunolabeling of the HSV-1-infected cells was done using monoclonal antibodies against three different nucleoporins (Nup62, Nup90, and Nup152) (Mab414; Covance, Berkeley, CA) at a dilution of 1:1,000 or against Nup153 (Abcam, Cambridge, United Kingdom) at a dilution of 1:250. After three washes with PBST plus 0.3% low-fat milk, cells were incubated with secondary anti-mouse antibodies (Alexa 488; Molecular Probes, Eugene, OR) at a dilution of 1:500. To ascertain infectivity, cells were labeled with antibodies against the tegument protein VP16 (a gift from B. Roizman, Chicago, IL) at a dilution of 1:1,000, followed by secondary anti-rabbit antibodies (Alexa 594; Molecular Probes) at a dilution of 1:500. After staining of nuclei with 4′,6′-diamidino-2-phenylindole (DAPI) (Roche, Mannheim, Germany), cells were embedded in fluorescence mounting medium (DakoCytomation, Glostrup, Denmark) and analyzed using a confocal laser scanning microscope (SP2; Leica, Wetzlar, Germany). Images were deconvolved by employing a blind deconvolution algorithm using the program suite Huygens Essential (SVI, Hilversum, The Netherlands).

Quantitative analysis. To estimate the distribution of nuclear pores, the numbers of pores on 10 nuclei of HeLa cells were counted on FESEM and cryo-FESEM images in mock- or HSV-1-infected cells incubated for 15 h. The interpore distances between two neighboring pores and the interpore areas bound by four to eight pores were then measured using AnalySIS Five software (Olympus, Hamburg, Germany). To estimate the approximate intensity of budding capsids, the numbers of budding capsids were counted on the nuclear surface at 8, 10, and 15 h of infection. Nuclei of HeLa cells grown as monolayers are triaxial ellipsoids. Therefore, nuclear volume (V) and nuclear surface (S) were calculated on the basis of the half axes (a, b, and c) measured on deconvolved confocal DAPI-stained images according to the following equations:

$$V = \frac{4}{3}\pi abc \quad \text{and} \quad S = 2\pi c^2 + 2\pi ab \int_0^1 \frac{1 - u^2 v^2 x^2}{\sqrt{1 - u^2 x^2}\ \sqrt{1 - v^2 x^2}}\, dx,$$

$$\text{whereby} \quad u = \frac{\sqrt{a^2 - c^2}}{a} \quad \text{and} \quad v = \frac{\sqrt{b^2 - c^2}}{b}$$

The numbers of pores and the maximal number of budding capsids per mean nuclear surface area were then calculated. In addition, numbers of nuclear pores were also estimated after immunolabeling of NPCs on deconvolved confocal images employing AnalySIS Five software. Numbers of pores, interpore distances, and interpore areas were compared by the Student t test.

Polyacrylamide gel electrophoresis and immunoblotting. HeLa cells were grown in 25-cm^2 cell culture flasks. Cells were infected with HSV-1 at an MOI of 2 and incubated at 37°C for 8, 10, 12, and 24 h. The protein extraction was accomplished as follows. After washing with phosphate-buffered saline, the cells were trypsinized and centrifuged at 800 × *g* for 5 min. The cell pellets were resuspended in protein extraction buffer (50 mM Tris-HCl [pH 7.4], 150 mM NaCl, 1 mM phenylmethylsulfonyl fluoride, 1 mM EDTA, 1% Triton X-100, 1% Na-deoxycholate, 1 μg/ml aprotinin, 1 mg/ml leupeptin, 0.1% sodium dodecyl sulfate [SDS]) for 20 min on ice and centrifuged at 10,000 × *g* for 5 min at 4°C. The supernatant was transferred into Eppendorf tubes, and the protein concentration was determined based on the method of Bradford (5a). After the addition of protein lysis buffer (0.5 M Tris-HCl [pH 6.8], 4.4% SDS, 1% β-mercaptoethanol, 20% glycerol, 1% bromphenol blue, H_2O), the samples were boiled for 5 min. Ten micrograms of protein from each sample was separated on a 6% SDS-polyacrylamide gel. After electrophoresis at 100 V for 2 h, the gel was transferred onto a polyvinylidene difluoride membrane. Blots were blocked with 5% low-fat milk in H-PBST (50 mM sodium phosphate buffer containing 155 mM NaCl, 0.05% Tween 20, and 10 mM HEPES) overnight. Subsequently, blots were probed with a 1:5,000 dilution of Mab414 (Covance, Berkeley, CA) in H-PBST. After two washing steps with H-PBST, blots were incubated with a 1:30,000 dilution of horseradish peroxidase-

TABLE 1. Data for HSV-1- and mock-infected cells[a]

Assay and infection type	No. of pores/ μm^2	Mean NPC diam (nm) (SD)	Mean NPC channel size (nm) (SD)	Mean interpore distance (nm) (SD)	Minimal interpore distance (nm) (SD)	Maximal interpore distance (nm)	Mean interpore area (nm^2) (SD)	Minimal interpore area (nm^2)	Maximal interpore area (nm^2)	Mean virion diam (nm) in PNS (SD)
FESEM										
HSV-1	6.5* (0.51)	198* (22.3)	92* (28.5)							
Mock	29.1 (2.0)	135 (12.1)	24.7 (14.7)							
Cryo-FESEM										
HSV-1	4.7* (1.36)			364** (63.6)	25.8	1,307	398,645* (64,030)	12,800	6,131,553	194 (29.6)
Mock	10.6 (1.56)			208 (14.4)	6.7	847	206,198 (16,000)	11,569	681,559	

[a] Shown are mean numbers and standard deviations (in parentheses) of nuclear pores per μm^2 nuclear surface, mean interpore distances, and mean interpore areas of HSV-1- and of mock-infected cells analyzed on images obtained by FESEM after in situ dry fracturing and/or by cryo-FESEM after rapid freezing and freeze etching of cell suspensions and mean viral diameter in the perinuclear space (PNS) measured on CFTEM images. Means are statistically different (*, $P < 0.001$; **, $P < 0.05$; number of nuclei = 10) compared to mock infected cells.

conjugated anti-mouse secondary antibodies (Sigma-Aldrich, Buchs, Switzerland). Blots were visualized on X-ray film using chemiluminescence.

RESULTS

Nuclear pore number declines during HSV-1 infection. The most prominent structures of the nuclear envelope are the nuclear pores. They may exhibit a distinctly nonrandom distribution over the nuclear surface with a minimum interpore distance that possibly influences their distribution (30). In some cells, nuclear pores occur in regular geometric arrays (11); in others, such as 3T3 cells, no indications of regular distributions were found (26). The densities of pores per unit area of the nuclear envelope vary considerably among different cells. A general value for higher eukaryotic cells is 10 to 20 pores/μm^2 (29), giving a total number of 3,000 to 4,000 pores per nucleus in somatic cells (16). However, only 1,900 pores were detected on 3T3 cell nuclei by confocal microscopy (26). The numbers of nuclear pores in HSV-1- and mock-infected HeLa cells on 10 images obtained after dry fracturing and freeze fracturing, respectively, at 15 h of incubation were counted. In mock-infected cells, the mean number was 10.7 pores/μm^2 nuclear surface in freeze-fractured cells and 29.1 pores/μm^2 nuclear surface in dry-fractured cells (Table 1). The difference of more than a factor of 2 is probably due to shrinkage occurring during fixation, permeabilization, dehydration, and drying. The mean numbers of pores in HSV-1-infected cells were 6.7 pores/μm^2 nuclear surface in freeze-fractured cells and 4.7 pores/μm^2 nuclear surface in dry-fractured cells (Table 1), which are 4.3 and 2.3 times lower, respectively, than values for mock-infected cells. This discrepancy possibly occurred because nuclear pores were altered in HSV-1-infected cells (see below), and thus, their identification in dry-fractured cells was difficult or even impossible.

Nuclei of HeLa cells are ellipsoids. The volume of ellipsoid nuclei in HEp-2 cells was reported to increase up to a factor of 2 in the course of HSV-1 infection (48). Therefore, we calculated the nuclear volume on the basis of the axes measured on confocal images after three-dimensional reconstruction. Surprisingly, the mean volume in HSV-1-infected cells at 15 h of incubation was larger than the nuclear volume in mock-infected cells only by a factor of 1.5 (Fig. 1). An increase in the volume of an ellipsoid by a factor of 1.5 results in an enlargement of its surface by a factor of ~1.31. Calculation of the nuclear surface on the basis of the measured axes in confocal images revealed mean surface areas of 450 μm^2 in mock-infected cells and of 480 μm^2 in HSV-1-infected cells. This increment by a factor of 1.06 is somewhat lower than the expected enlargement and is probably related to methodological errors. Calculation of the mean number of pores counted on cryo-FESEM images per the total nuclear surface area obtained from confocal images revealed a mean of 4,800 pores/nucleus in mock-infected cells but only a mean of 2,250 pores/nucleus in HSV-1-infected cells, suggesting that the number of pores declined by a factor of 2.1 within 15 h of incubation. The mean pore numbers identified by immunostaining irrespective of the antibodies used were about 2,000 in mock-infected cells and 1,560 in HSV-1-infected cells. Estimation of numbers of pores in cryo-FESEM images might result in overestimation because the spherical surface of the nucleus cannot be satisfactorily considered. On the other hand, estimation of pore numbers in fluorescent images probably results in underestimation because the resolution power is not sufficient to allow a clear separation of two pores lying closer together than its diameter. Enlargement of pores (see below) will also contribute to underestimations. Nevertheless, the

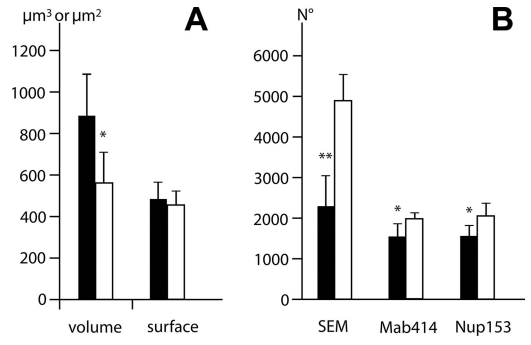

FIG. 1. (A) Means and standard deviations of nuclear volume and nuclear surface of HSV-1-infected (■) and mock-infected (□) cells calculated on the basis of the half axes measured on confocal images. (B) The number of nuclear pores counted on cryo-FESEM images (NP-SEM) were calculated per nuclear surface of confocal images, and the mean number of fluorescent signals was determined on nuclei labeled with Mab414 (NP-414) or with antibodies against Nup153 (NP-153) as described in Materials and Methods. Means are statistically different (*, $P < 0.05$; **, $P < 0.001$; number of nuclei = 10) compared to mock-infected cells.

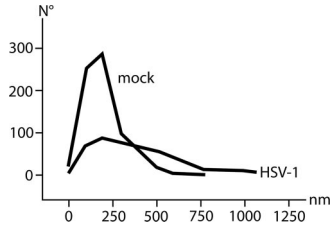

FIG. 2. Frequency distribution of the interpore distance in 10 HSV-1- and 10 mock-infected cells measured on cryo-FESEM images (60 distances on average). The mean interpore distance is 364 nm in HSV-1-infected cells and 208 nm in mock-infected cells.

mean number of pores in HSV-1-infected cells was lower than that in mock-infected cells by a factor of 1.8, which corresponds to the data from cryo-FESEM and thus strongly supports the idea of decrement of pore numbers in the course of HSV-1 infection. To get an idea about nuclear pore distribution, we measured the interpore distances in cryo-FESEM images. As shown in Fig. 2, the mean interpore distance varied considerably in HSV-1-infected cells compared to that in mock-infected cells. The mean interpore distance in HSV-1-infected cells was larger than that in mock-infected cells by a factor of 1.75 (Table 1). The diverse numbers of nuclear pores and the difference in distributions in mock-infected cells and HSV-1-infected cells are readily obvious in cryo-FESEM images (Fig. 3A to E).

Nuclear pores dilate in HSV-1-infected cells. NPCs form a key transport barrier between the cytoplasm and the nucleus. In nondividing cells, nucleocytoplasmic shuttling of macromolecules is tightly controlled by their selective translocation through the 30- to 50-nm-long (52) and 9-nm-wide (36) NPC central channel. This channel was shown to be expandable, enabling the transport of macromolecules with diameters of up to ~39 nm (38). Pores with a central channel of 35 to 45 nm were found in dry-fractured *Xenopus* egg nuclei (15). To illuminate whether infection with HSV-1 may induce alterations of nuclear pore complexes per se, as suggested previously (27), we imaged nuclear pores of dry-fractured nuclei at higher magnifications (Fig. 3F to H). Mea-

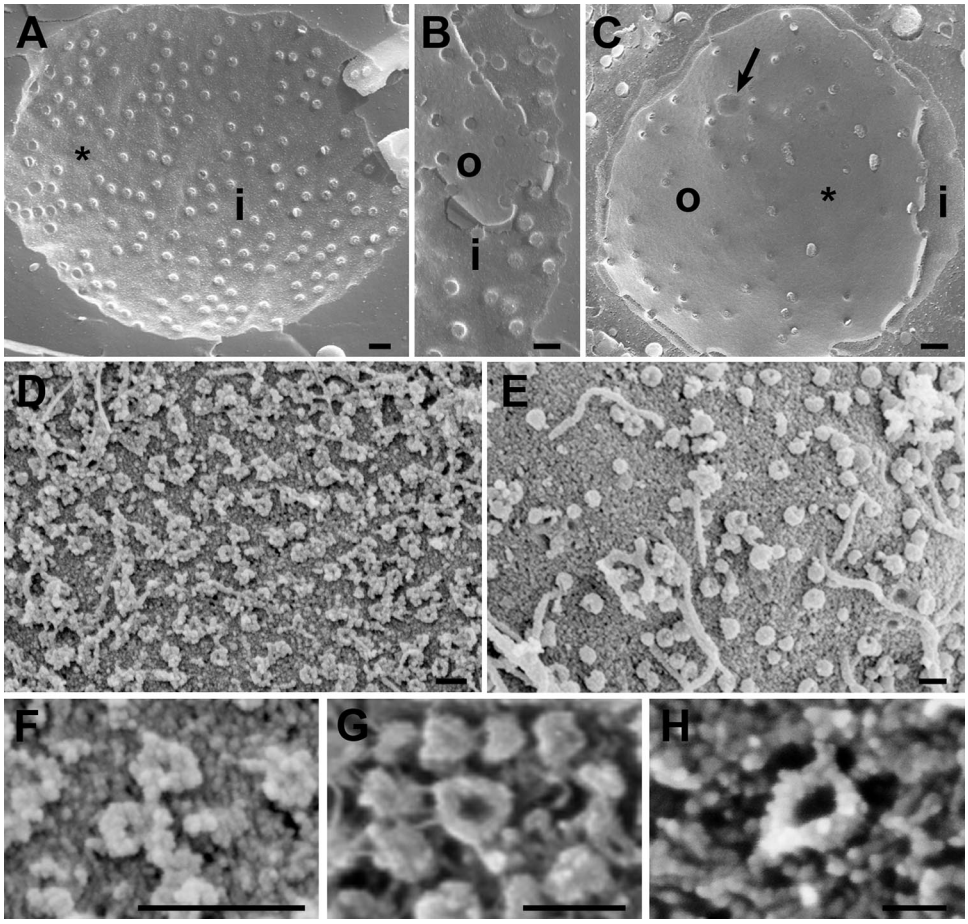

FIG. 3. Images of nuclear surfaces of mock- and HSV-1-infected Vero cells (A to C) and HeLa cells (D to H) 15 h postinfection obtained by cryo-FESEM after freeze fracturing (A to C) or by FESEM after dry fracturing (D to H) showing remarkable reductions in the number of nuclear pores/μm^2 and enlargement of the maximal interpore area (asterisks) in HSV-1-infected cells (C and E) compared to mock-infected cells (A and D). Nuclear pores appear on the inner nuclear membrane (i) as round buttons but as a distinct low depression at the outer nuclear membrane (o) in mock-infected cells (A and B). In HSV-1-infected cells, the NPC and/or nuclear material protrudes through normal-sized and enlarged nuclear pores, and a distinctly bordered hole (arrow) was formed as apparent at the outer nuclear surface (C). The overall diameter of the NPC is enlarged and the central pore channel is dilated in dry-fractured HSV-1-infected cells (G and H) compared to NPCs of mock-infected cells (F). Bars, 200 nm.

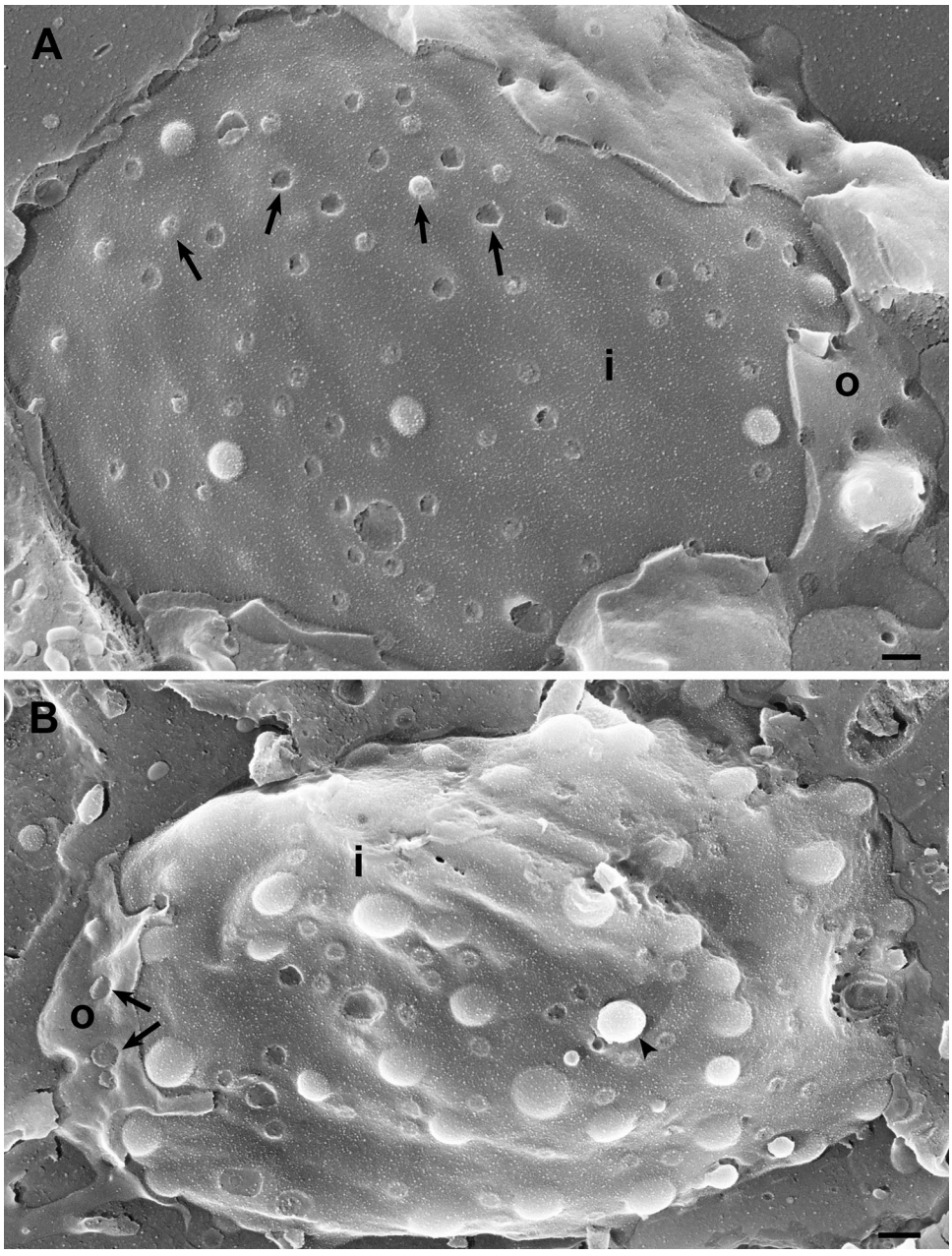

FIG. 4. Cryo-FESEM images showing the inner (i) and parts of the outer (o) nuclear membranes of HSV-1-infected HeLa cells at 10 h of incubation. (A) Nuclear pores appear as button-like structures or holes. There are also slightly larger holes with distinct borders and small protrusions of similar size (arrows) as well as three holes with diameters of up to 250 nm and a few budding capsids. (B) The number of budding capsids is about 1.8/μm^2. One budding is probably close to completion (arrowhead). There are holes from 110 to 220 nm, two protrusions (arrows) of 130 nm in diameter, and folds of the nuclear surface. Bars, 200 nm.

surements of about 400 pores on 10 different nuclei revealed the mean central channel diameter to be 28.7 nm in mock-infected cells. The mean central channel diameter in HSV-1-infected nuclei, however, was 92 nm. The overall diameter of nuclear pores was 135 nm in mock-infected cells but was 198 nm in HSV-1-infected cells (Table 1) at 15 h of incubation.

The appearance of nuclear pores in frozen-hydrated nuclei depends largely on the fracture plane (55). They look like round indentations at the outer nuclear membrane but button-like structures at the inner nuclear membrane. In freeze-fractured, mock-infected cells, nuclear pores also appeared mostly as small button-like structures at the inner nuclear membrane with an average diameter of 120 nm or, occasionally, as holes of similar diameters (Fig. 3A and B). The appearance of nuclear pores at the inner nuclear membrane in HSV-1-infected cells was heterogeneous. They either were similar to those in mock-infected cells or appeared as small protrusions or as holes with diameters of 140 to 160 nm. In addition, holes with diameters of up to 220 nm were found at the inner nuclear membrane (Fig. 4). Nuclear pores of mock-infected cells at the

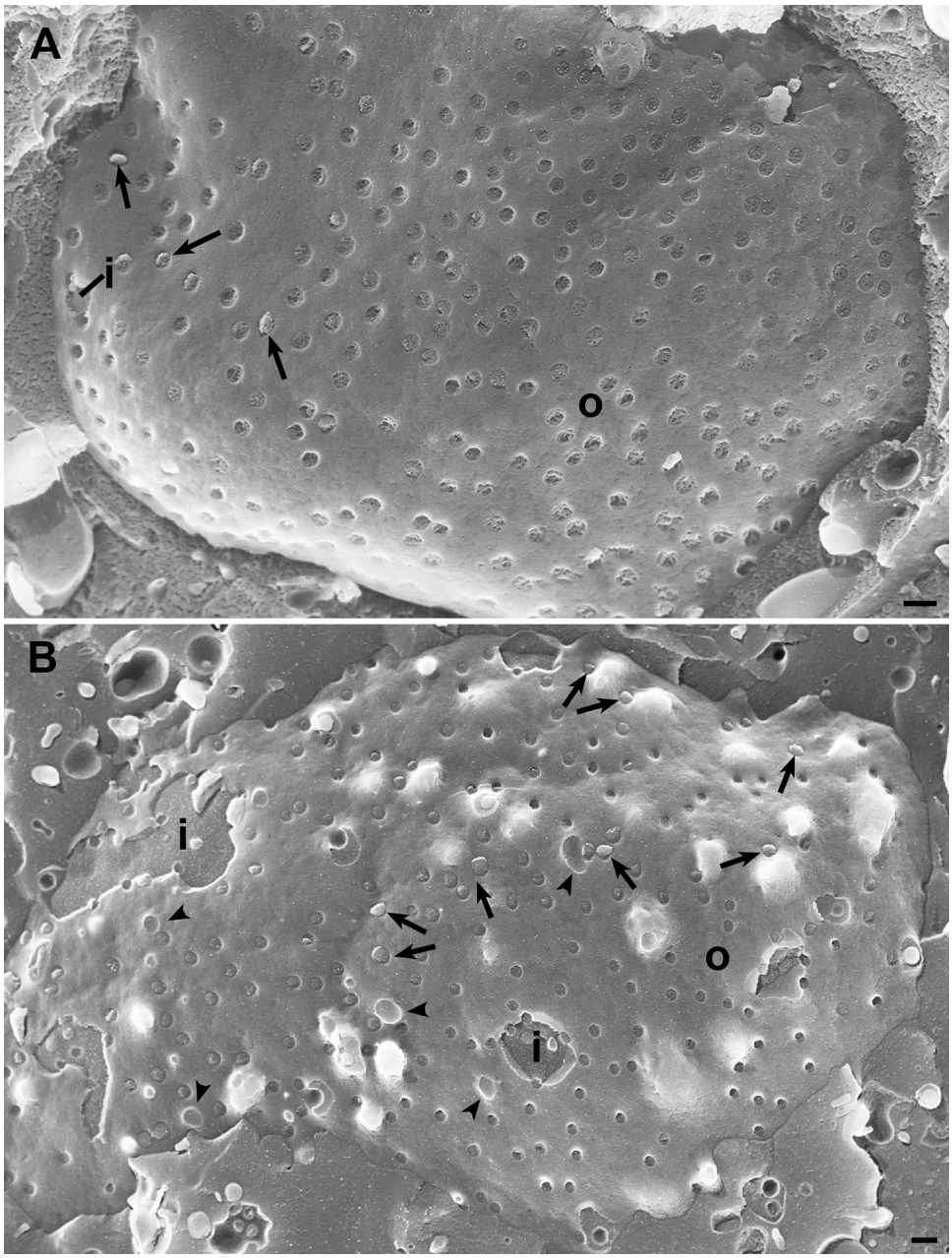

FIG. 5. Cryo-FESEM images of the outer nuclear membrane (o) of mock-infected (A) and HSV-1-infected (B) HeLa cells after 10 h of incubation. (A) Nuclear pores appear as round, small depressions with a distinct NPC structure, and a few appear as small buttons (arrows). (B) Pores appear either as small but deep depressions without obvious NPC structure or as buttons. Some of them have larger diameters and are over top the nuclear membrane (arrows). In addition, there are holes with distinct borders (arrowheads) and numerous budding capsids. The outer nuclear membrane is locally broken away, giving view to the inner nuclear membrane (i). Bars, 200 nm.

outer nuclear membrane were visible as low round depressions with a mean diameter of 120 nm and clear NPC structure, which occasionally filled the pores entirely (Fig. 5A). In HSV-1-infected cells, most of the nuclear pores appeared either as distinct depressions missing NPC structures or as distinct small protrusions (Fig. 5B and 6) with diameters of 120 to 130 nm at the outer nuclear membrane. There were also larger protrusions with diameters at the base of 140 to 310 nm and holes with diameters of up to 270 nm. Protrusions of any size were distinctly bordered at the base, resembling the bordering of nuclear pores.

The question of whether or not the larger protrusions and holes at the nuclear surface are related to nuclear pores can best be answered by examining fracture planes or thin sections perpendicular through these protrusions or holes. Fracture planes obtained by freeze fracturing showed gaps in the nuclear envelope distinctly bordered by intact outer and inner nuclear membranes (Fig. 7B). Such gaps had measured diam-

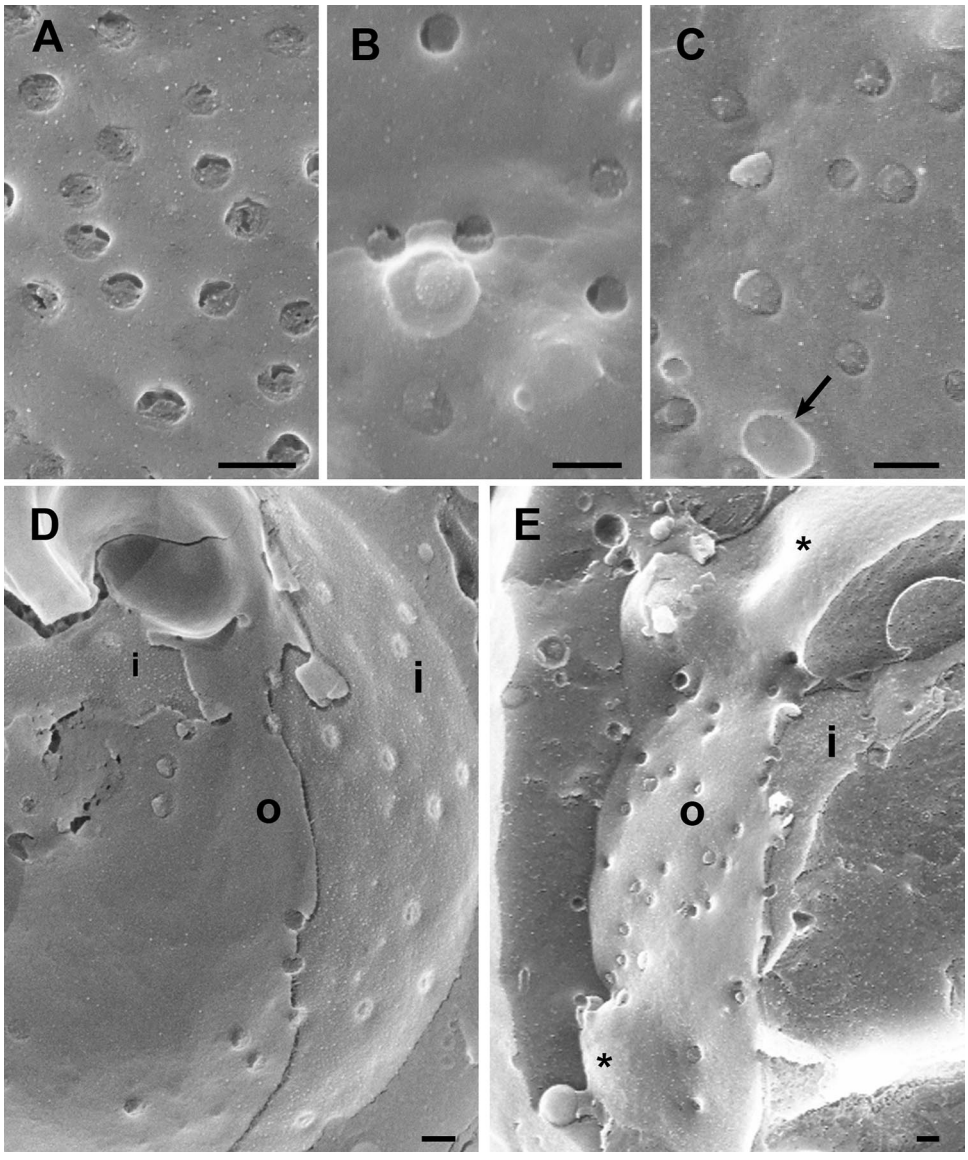

FIG. 6. Details of the outer nuclear membrane shown in Fig. 3 (A to C) and cryo-FESEM images of HSV-1-infected Vero cells after 10 h (D) and 17 h (E) of incubation. (A) Nuclear pores of mock-infected cells with NPC structures. (B and C) Nuclear pores either miss NPC structures or are completely filled with NPCs and/or nuclear material that protrudes into the cytoplasm of HSV-1-infected cells. The hole (arrow) does not give a view onto the inner nuclear membrane. (D) Large areas are devoid of nuclear pores, the number of which is low, and appear as buttons at both the inner (i) and outer (o) nuclear membranes. (E) Large areas (asterisks) devoid of pores bulge into the cytoplasm. Bars, 200 nm.

eters of up to 560 nm. Imaging of the nuclear surface on thin sections obtained after rapid freezing and freeze substitution in situ also revealed gaps distinctly bordered by nuclear membranes, suggesting that they were dilated nuclear pores (Fig. 7C and D). Nuclear material containing capsids was found to protrude through large holes into the cytoplasm. It never merged with the cytoplasmic matrix (Fig. 7E). The distribution of intact and impaired nuclear pores per μm^2 is presented in Fig. 8, showing that only 40% of the nuclear pores in HSV-1-infected cells were intact, while in mock-infected cells, nearly all pores were intact.

Budding capsids require membranes. The main event at the nuclear surface in HSV-1-infected cells is expected to be the budding of capsids. The result of a capsid budding at the inner nuclear membrane is an enveloped virion (44) with a diameter of about 200 nm (Table 1 and Fig. 9). These virions can accumulate in the perinuclear space (7, 49). Assuming that virions are sphere-like particles (18), the surface area of a single virion equals ~125,000 nm^2. The approximate mean interpore area between neighboring pores was 206,198 nm^2 in mock-infected cells. The maximal interpore area was about 681,500 nm^2, and the minimal interpore area was 11,600 nm^2. A capsid budding requires 125,000 nm^2 from the inner nuclear membrane; i.e., it reduces the nuclear surface by 125,000 nm^2. Surprisingly, the mean interpore area measured in HSV-1-infected cells 15 h postinfection was larger than that in mock-infected cells by close to a factor of 2 (Table 1). The maximal interpore area was even 10 times larger than that in mock-infected cells, whereas the minimal interpore areas were

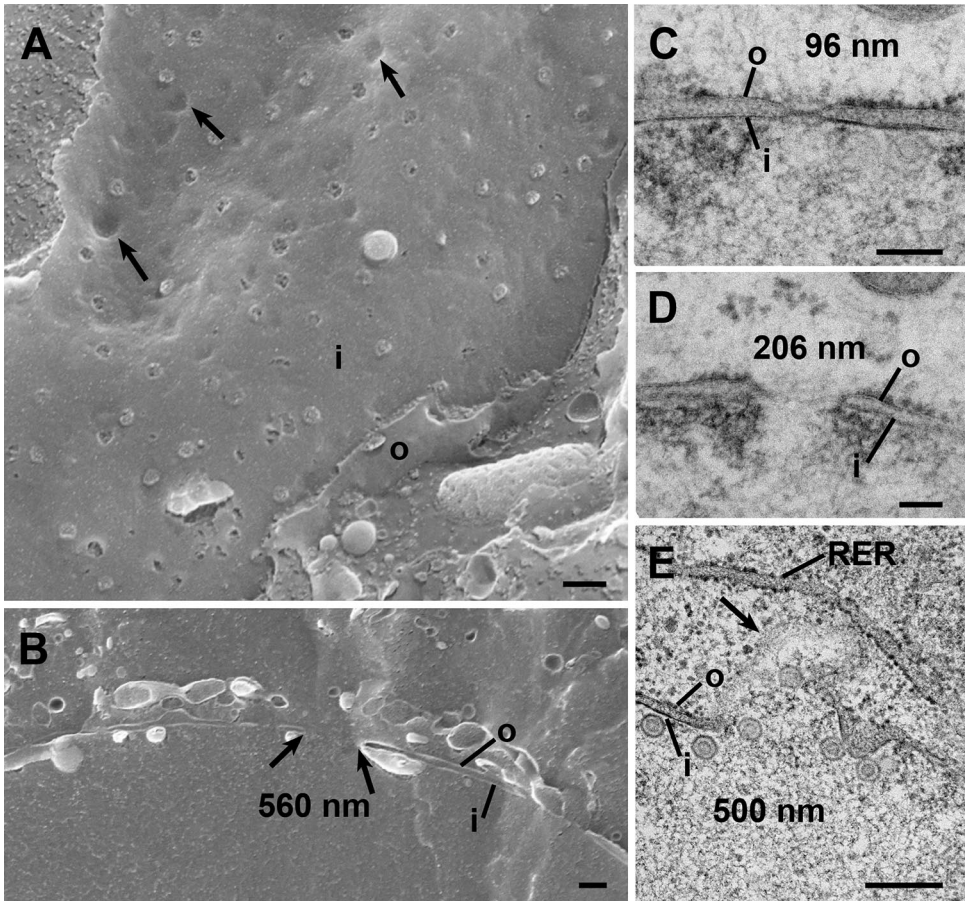

FIG. 7. Cryo-FESEM and CFTEM images of HSV-1-infected Vero cells at 15 h (A) and 17 h (B to E) of infection. (A) Inner nuclear membrane (i) with a single budding capsid, normal-sized nuclear pores with material protruding through some of them, and indentations (arrows) with a smooth transition to the inner nuclear membrane indicating that these resulted from budding. (B) Cross-fracture plane through a nucleus showing a gap of 560 nm bound by the inner (i) and outer (o) nuclear membranes. (C to E) CFTEM images of a normal nuclear pore with clearly visible pore complex (C), a gap with boundaries formed by the inner and outer nuclear membranes (D), and nuclear material (arrow) together with capsids protruding through a gap into the cytoplasm close to an RER cisterna. Bars, 200 nm.

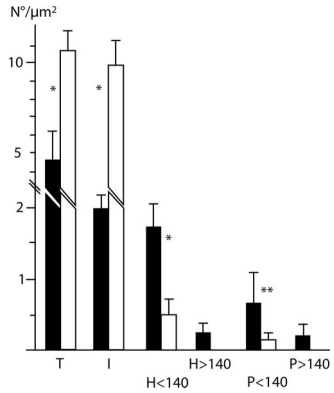

FIG. 8. Means and standard deviations of intact and impaired nuclear pore numbers expressed per μm^2 nuclear surface in HSV-1-infected (■) and mock-infected (□) cells incubated for 15 h analyzed on cryo-FESEM images. T, total pores; I, intact pores; H < 140 and P < 140, holes and pores <140 nm in diameter, respectively; H > 140 and P > 140, holes and pores >140 nm in diameter, respectively. Data for each morphological entity were compared by the Student *t* test (*, $P < 0.0001$; **, $P < 0.05$; $n = 10$).

similar in mock- and HSV-1-infected cells. These data suggest highly dynamic processes taking place at the nuclear envelope in the course of the nuclear exit of capsids, leading to an enlargement of the interpore area. Indeed, a maximum of 1.83 capsids per 1 μm^2 nuclear surface area were found to bud (Fig. 10), requiring 228,750 $nm^2/\mu m^2$, or 22.8%. By expressing the number of budding capsids per the entire nuclear surface of 450 to 480 μm^2, a total number of 823 to 878 capsids will bud more or less simultaneously provided that budding activity is evenly distributed over the entire nuclear surface. If this assumption was correct, a total area of 103 to 109 μm^2 of the inner nuclear membrane would be required to provide enough membranes for budding at 10 h of infection. Interestingly, high budding activity ($1.83/\mu m^2$) was found at 10 h of incubation (Fig. 4B and 5B), but low activity ($<0.1/\mu m^2$) was found at 15 h postinfection (Fig. 10). However, at 15 h postinfection, indentations at the nuclear surface with diameters of 120 to 160 nm were found (Fig. 7A). This smooth transition from the concavity into the inner nuclear membrane suggests that they are related to budding because the inner membrane is pulled behind the budding capsid for fission of the enveloped virions, resulting in an indentation (59).

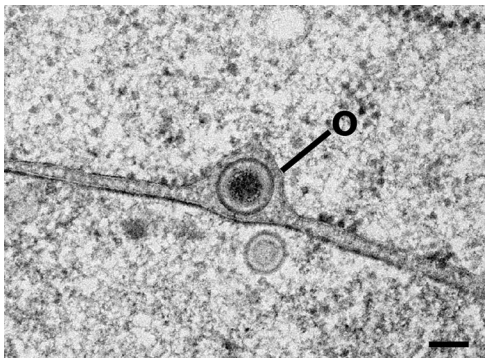

FIG. 9. CFTEM micrograph of a Vero cell at 12 h of infection showing an enveloped virion within the perinuclear space forcing the outer nuclear membrane (o) into the cytoplasm. Bar, 100 nm.

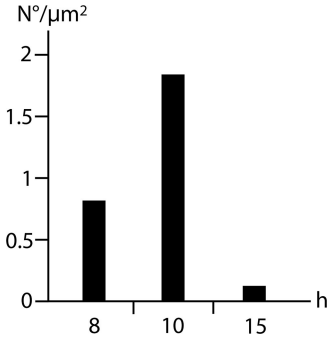

FIG. 10. Number of budding capsids per μm^2 at the nuclear envelope at 8, 10, and 15 h of incubation.

Nucleoporins are irregularly distributed in HSV-1-infected cells. Electron microscopy provided clear evidence for dramatic alterations of nuclear pore structure and distribution. Nuclear pore alterations may correlate with the degradation of nucleoporins, as was seen in cells infected with poliovirus (19, 20). In order to determine possible changes in the distribution of nucleoporins in the course of HSV-1 infection, cells were immunolabeled using antibodies against Nup62, Nup90, and Nup152 (Mab414) or Nup153. To ascertain HSV-1 infection, cells were immunolabeled using antibodies against the tegument protein VP16. Cells were analyzed using a confocal laser scanning microscope.

Under carefully controlled and favorable conditions, the resolution of the confocal microscope was claimed to be sufficient to visualize single NPC-sized particles and to distinguish between single particles and particle aggregates (25). In this study, mock-infected cells exhibited disseminated nucleoporins at all times examined (Fig. 11A). However, the fluorescence signals could not be resolved into single NPCs because of the irregular density and variation in size. Even the rather regular pattern in mock-infected cells could not be resolved into single NPCs because of the large number of signals. First, changes became apparent as early as 8 h postinoculation in HSV-1-infected cells. Nucleoporins labeled with Mab414 (Fig. 11B and C) or Nup153 (Fig. 11D) showed irregular distribution, focal enhancement, and a reduced number of fluorescence signals that were quantified. There was no significant difference in numbers of signals detected between Mab414 (recognizing Nup62, Nup90, and Nup152) and the antibodies against Nup153. The significantly lower number of signals ($P < 0.05$) in HSV-1-infected cells than that in mock-infected cells, as shown in Fig. 1, and the irregular distribution of labeled NPC confirm the data drawn from cryo-FESEM images showing that nuclear pore numbers decline and pore distribution alters in the course of HSV-1 infection.

Nucleoporins do not disappear from cells. Nup153 was shown to be downregulated in HSV-1-infected cells (42). This and the lower frequency of fluorescent signals prompted us to analyze nucleoporins by Western blots. The results obtained with HSV-1-infected cells at any time of incubation were similar to those obtained with mock-infected cells (Fig. 12), suggesting that nucleoporins do not disappear but are rather disseminated into the cytoplasm in the course of HSV-1 infection.

DISCUSSION

Nuclear size has been reported to increase in HEp-2 cells infected with HSV-1 (48) to a twofold larger volume, which is correlated to the formation of extrachromosomal compartments (35). Nuclear enlargement implies the insertion of membrane constituents and/or the formation of additional nuclear pores to guarantee the integrity of the nuclear envelope. The shape of the nucleus of HeLa and Vero cells is like an ellipsoid with a short c axis in situ. A twofold increase in nuclear volume would result in an enlargement of the nuclear surface by a factor of ~1.6. However, the mean volume increased only by a factor of 1.5, and the nuclear surface was enlarged by a factor of 1.06, which is slightly lower than the theoretically expected enlargement of the nuclear surface, by a factor of ~1.31. The difference between volume increment in HEp-2 cells and that in HeLa cells may be due to physiological properties. Alternatively, the nuclear volume in HEp-2 cells was estimated on the basis of the a and b axes only (48). We, however, used all three axes of third-dimension-reconstructed cells, which leads to more accurate results, at least in mathematical terms. The mean interpore area determined with cryo-FESEM images was enlarged by a factor of 2, and the mean number of nuclear pores was lower by a factor of 2.1 at 15 h of incubation, suggesting a loss of nuclear pores. Additional enlargement of the mean interpore area could be due a dislocation of nuclear pores. To achieve such large nuclear pore-free areas, dislocation would lead to the accumulation of pores at neighboring sites, which was not the case.

Negatively stained nuclear pores on the surface of a carbon-coated copper grids measure 125 nm in diameter and are occupied by the NPC (57), which controls the nuclear import and export of proteins up to 39 nm in diameter (38). In ultrathin sections where nuclear membranes were hit perpendicular to the nuclear surface, details of both nuclear membranes and nuclear pores could be visualized by CFTEM. Intact nuclear pores measured 100 to 110 nm in diameter. The discrepancy in pore size between the two different preparation techniques is due to section thickness that does not allow precise measurements and possibly to shrinking artifacts. Pore diameters measured on images obtained by cryo-FESEM varied between 110 and 130 nm in mock-infected cells. In HSV-1-infected cells, they measured up to 160 nm. In addition, holes in the nuclear envelope were found to be up to 560 nm in diameter by cryo-FESEM. Nuclear material protruded through some of these

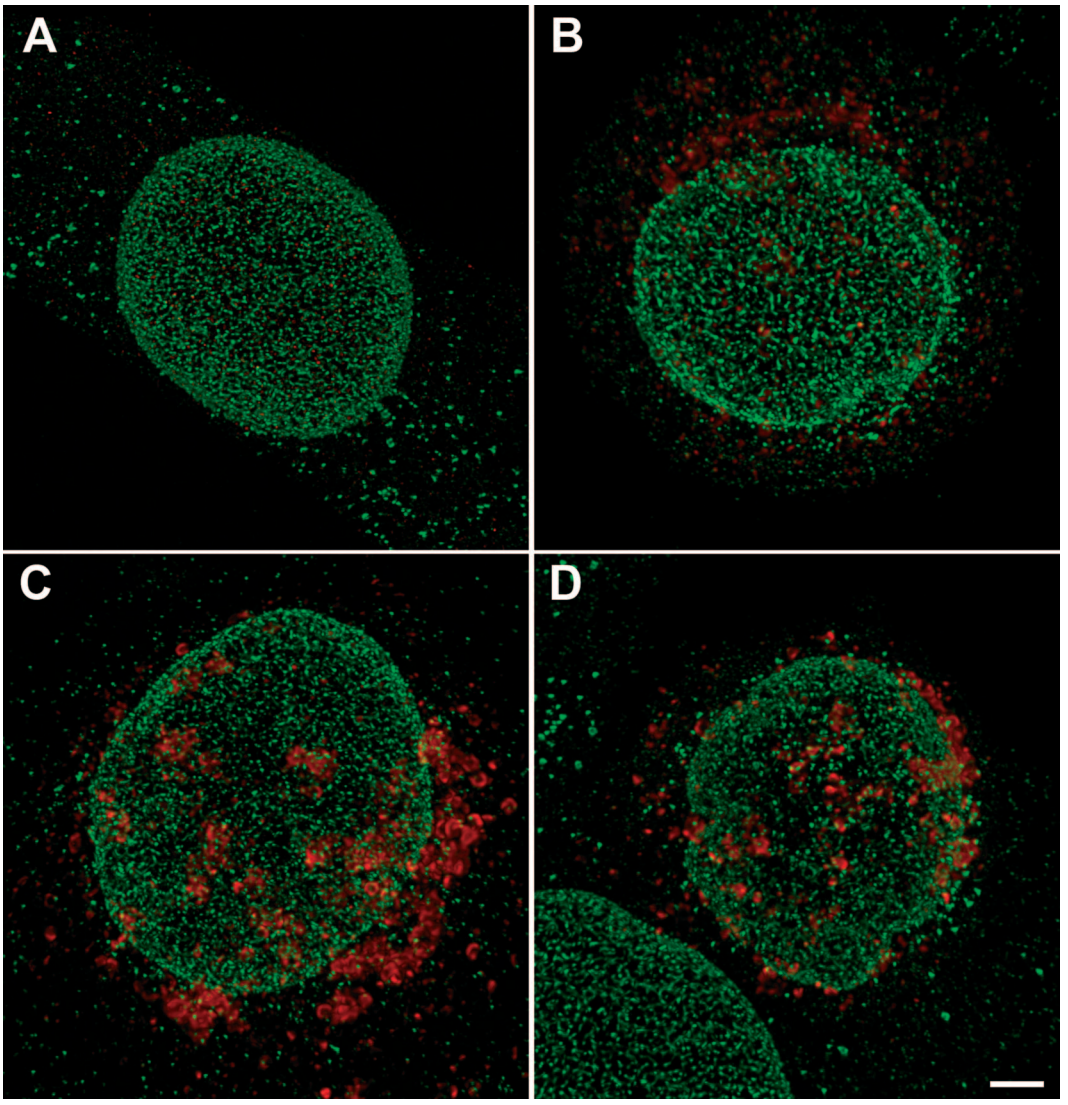

FIG. 11. Confocal microscopic images of mock-infected cell at 15 h (A) and of HSV-1-infected HeLa cells recognized by staining of the tegument protein VP16 (red) at 8 h (B) or 15 h (C and D) postinoculation immunostained for nucleoporins (green) with Mab414 (A, B, and C) or Nup153 (D). Nucleoporin distribution is regular in mock-infected cells when stained with Mab414 (A) or with Nup153 (not shown). In HSV-1-infected cells, nucleoporin distribution is irregular, the fluorescence signal is focally enhanced, and the number of signals is reduced, as apparent at 15 h of incubation (C and D). Bar, 1 μm.

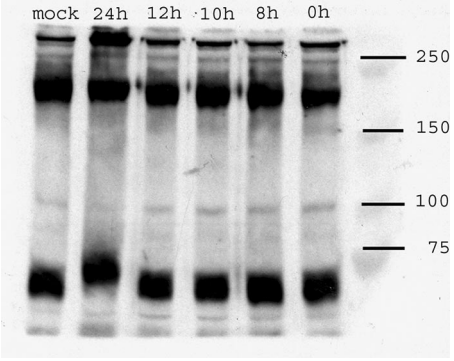

FIG. 12. Western blots of mock- and HSV-1-infected HeLa cells 0 to 24 h postinoculation as described in Materials and Methods using Mab414 showing no apparent differences between mock- and HSV-1-infected cells at any time of infection.

holes, as was confirmed by CFTEM in thin sections through cells fixed and processed in situ. Such protrusions were also reported for cells infected with bovine herpesvirus 1 (BHV-1) but were falsely interpreted as being budding capsids (59). The distinct border by the nuclear membranes and the round shape strongly suggest that these holes are dilated nuclear pores. Fracture planes and sections through pores and holes support this idea. The presence of capsids within nuclear material protruding through such holes into the cytoplasmic matrix (Fig. 7E) led to the suggestion that capsids may use these holes as gateways to gain direct access to the cytoplasmic matrix (59). The same idea was reported previously for the release of capsids of simian agent 8 (6). Holes that are not filled with protruding nuclear material are probably the result of the fracture plane running at the base of the protrusions so that the protruding material was removed during fracturing. The same

could have led to the empty nuclear pores at the inner nuclear membrane. Unfortunately, NPCs could not be visualized in more detail by cryo-FESEM. Frozen structures rapidly undergo beam damage during imaging. Either NPCs were removed during fracturing or the entire pore was filled, making an exact distinction between NPC structure and other material extremely difficult. However, by employing in situ preparations by fixation, drying, and fracturing at ambient temperatures, almost all cytoplasmic components and nuclear membranes were removed, giving a clear view onto the nuclear pore complex. Images of nuclei prepared according to a previously described protocol (3) clearly showed enlarged nuclear pore complexes with an enlarged central channel, suggesting an impairment of nuclear pores without a complete loss of NPC proteins through which capsids may exit the nucleus. While our data do not contradict the nuclear pore egress model, they also cannot give final proof of it. For that purpose, further studies toward the identification of capsid exporters will have to be done.

The overall vertebrate NPC structure comprises the spoke-ring complex, which encircles the central channel complex called the transporter. The spoke complex is framed by the cytoplasmic ring and the nuclear ring, which serve as attachment sites for the cytoplasmic filaments and the nuclear basket, respectively (53, 62). Nup62 is located at the cytoplasmic entry side of the transporter (47). Locations of Nup90 and Nup152 are not defined to our knowledge. Nup153 is part of the nuclear basket (37, 39). Nup153 is known to be required for NPC assembly and anchoring of the NPC to the nuclear envelope (12) but is also involved in nuclear import and export (5). Nup153 was shown to be downregulated in HSV-1-infected cells (42). Proteins such as capsid proteins and tegument proteins have to be imported into the nucleus for HSV-1 replication. The question arises whether nuclear import is affected in HSV-1-infected cells. In poliovirus-infected HeLa cells, nuclear import was drastically inhibited in accordance with the degradation of NPC components (20). The number of intact pores in HSV-1-infected cells was ~2 pores/μm^2. The number of intact nuclear pores per entire nuclear surface equals a total of 960 at 15 h of infection, which might be sufficient to fulfill the requirements for nuclear import in HSV-1-infected cells. Furthermore, dilation of nuclear pores does not necessarily imply an impairment of nuclear import and export as long as nucleoporins are present. The nucleocytoplasmic barrier for molecules bigger than 70 kDa remained intact in HSV-1-infected Vero and Hep-2 cells (24), suggesting that the selectivity of nuclear import is not disturbed for large molecules at least.

Capsids escaping the nucleus by budding at the inner nuclear membrane require its membrane for envelope formation. The fate of these perinuclear virions is controversially discussed. Capsids are assumed to be deenveloped (49) by fusion of the viral envelope with the outer nuclear membrane. Consequently, the inner nuclear membrane would undergo constant reduction, whereas the outer nuclear membrane and the adjacent rough endoplasmic reticulum (RER) would get continually enlarged. To our knowledge, such deformations have never been described in this context. Conversely, one might assume that membrane constituents inserted into the outer nuclear membrane recycle back to the inner nuclear membrane so that a continuous flow would be maintained between inner and outer nuclear membranes and vice versa. Proof does not yet exist for this concept as well. However, the more profound crux of this concept remains in neglecting the fact that virions can accumulate in the perinuclear space (4, 7, 8, 27, 49, 50, 54) or can be transported into adjacent cisternae of the RER (13, 17, 41, 45, 51, 58, 61). Recently, it was proposed that perinuclear virions are transported via RER cisternae directly into Golgi cisternae; those membranes were shown to be connected to RER membranes (27, 61). In this context, the inner nuclear membrane would remain as the final viral envelope. In HSV-1 deleted of US3 (43) or of glycoprotein B (10), extremely large amounts of virions accumulate in the perinuclear space. The membranes of all these virions must be provided by a mechanism other than recycling. Furthermore, images obtained at 10 h of infection suggest that budding may take place simultaneously more or less all over the nuclear surface, even in the close vicinity of nuclear pores. Simultaneous budding of a maximal 1.8 capsids/μm^2 giving a total of more than 800 capsids would require a total amount of ~100 μm^2 of membranes that must be provided prior to and/or simultaneously to budding.

In conclusion, the data indicate a loss of nuclear pores, dilation of nuclear pores, and dilation of the central NPC channel through which capsids may escape to gain direct access to the cytoplasmic matrix. There, they may bud at Golgi membranes. The molecular mechanisms guiding the nuclear export of capsids via impaired nuclear pores still need to be identified. Nucleoporins are probably not completely lost in dilated nuclear pores, suggesting that nucleocytoplasmic transportation is not severely affected. The high budding activity as early as 10 h after infection requires a large amount of membranes. Hence, substantial amounts of membrane constituents need to be inserted into the inner nuclear membranes for viral envelope formation during the budding of capsids and for the maintenance of membrane integrity of enlarging nuclei. Whether or not these membrane constituents are translocated to the outer nuclear membrane by the fusion of the envelope of perinuclear virions and how exactly perinuclear virions are intraluminally transported via RER cisternae into Golgi cisternae remain to be verified.

ACKNOWLEDGMENTS

We thank Bernard Roizman for providing antibodies against VP16 and Jeanne Peter for drawing of graphs.

This study was supported by the Foundation for Scientific Research at the University of Zürich, Zürich, Switzerland.

REFERENCES

1. **Allen, T. D., G. R. Bennion, S. A. Rutherpord, S. Reipert, A. Ramalho, E. Kiseleva, and M. W. Goldberg.** 1997. Macromolecular substructure in nuclear pore complexes by in-lens field-emission scanning electron microscopy. Scanning **19:**403–410.
2. **Allen, T. D., and M. W. Goldberg.** 1993. High-resolution SEM in cell biology. Trends Cell Biol. **3:**205–208.
3. **Allen, T. D., S. A. Rutherford, G. R. Bennion, C. Wiese, S. Riepert, E. Kiseleva, and M. W. Goldberg.** 1998. Three-dimensional surface structure analysis of the nucleus. Methods Cell Biol. **53:**125–138.
4. **Baines, J. D., P. L. Ward, G. Campadelli-Fiume, and B. Roizman.** 1991. The U_L20 gene of herpes simplex virus 1 encodes a function necessary for viral egress. J. Virol. **65:**6414–6424.
5. **Ball, J. R., and K. S. Ullman.** 2005. Versatility at the nuclear pore complex: lessons learned from the nucleoporin Nup153. Chromosoma **114:**319–330.

5a. **Bradford, M. M.** 1976. A rapid and sensitive method for the quantitation of microgram quantities of protein utilizing the principle of protein-dye binding. Anal. Biochem. **72:**248–254.

6. **Borchers, K., and M. Oezel.** 1993. Simian agent 8 (SA8): morphogenesis and ultrastructure. Zentralbl. Bakteriol. **279:**526–536.
7. **Campadelli-Fiume, G., F. Farabegoli, S. Di Gaeta, and B. Roizman.** 1991. Origin of unenveloped capsids in the cytoplasm of cells infected with herpes simplex virus 1. J. Virol. **65:**1589–1595.
8. **Darlington, R. W., and L. H. Moss.** 1968. Herpesvirus envelopment. J. Virol. **2:**48–55.
9. **Fahrenkrog, B., J. Koser, and U. Aebi.** 2004. The nuclear pore complex: a jack of all trades? Trends Biochem. Sci. **29:**175–182.
10. **Farnsworth, A., T. W. Wisner, M. Webb, R. Roller, G. Cohen, R. Eisenberg, and D. C. Johnson.** 2007. Herpes simplex virus glycoproteins gB and gH function in fusion between the virion envelope and the outer nuclear membrane. Proc. Natl. Acad. Sci. USA **104:**10187–10192.
11. **Franke, W. W.** 1974. Structrure, biochemistry and functions of the nuclear envelope. Int. Rev. Cytol. Suppl. **4:**71–239.
12. **Gerace, L., and B. Burke.** 1988. Functional organization of the nuclear envelope. Annu. Rev. Cell Biol. **4:**335–374.
13. **Gilbert, R., K. Ghosh, L. Rasile, and H. P. Ghosh.** 1994. Membrane anchoring domain of herpes simplex virus glycoprotein gB is sufficient for nuclear envelope localization. J. Virol. **68:**2272–2285.
14. **Goldberg, M. W., and T. D. Allen.** 1995. Structural and functional organization of the nuclear envelope. Curr. Opin. Cell Biol. **7:**301–309.
15. **Goldberg, M. W., C. Wiese, T. D. Allen, and K. L. Wilson.** 1997. Dimples, pores, star-rings, and thin rings on growing nuclear envelopes: evidence for structural intermediates in nuclear pore complex assembly. J. Cell Sci. **110:** 409–420.
16. **Gorlich, D., and U. Kutay.** 1999. Transport between the cell nucleus and the cytoplasm. Annu. Rev. Cell Dev. Biol. **15:**607–660.
17. **Granzow, H., F. Weiland, A. Jons, B. G. Klupp, A. Karger, and T. C. Mettenleiter.** 1997. Ultrastructural analysis of the replication cycle of pseudorabies virus in cell culture: a reassessment. J. Virol. **71:**2072–2082.
18. **Grunewald, K., P. Desai, D. C. Winkler, J. B. Heymann, D. M. Belnap, W. Baumeister, and A. C. Steven.** 2003. Three-dimensional structure of herpes simplex virus from cryo-electron tomography. Science **302:**1396–1398.
19. **Gustin, K. E., and P. Sarnow.** 2001. Effects of poliovirus infection on nucleocytoplasmic trafficking and nuclear pore complex composition. EMBO J. **20:**240–249.
20. **Gustin, K. E., and P. Sarnow.** 2002. Inhibition of nuclear import and alteration of nuclear pore complex composition by rhinovirus. J. Virol. **76:**8787–8796.
21. **Hagiwara, A., Y. Fukazawa, M. Deguchi-Tawarada, T. Ohtsuka, and R. Shigemoto.** 2005. Differential distribution of release-related proteins in the hippocampal CA3 area as revealed by freeze-fracture replica labeling. J. Comp. Neurol. **489:**195–216.
22. **Haines, H., and R. J. Baerwald.** 1976. Nuclear membrane changes in herpes simplex virus-infected BHK-21 cells as seen by freeze-fracture. J. Virol. **17:**1038–1042.
23. **Hermann, R., and M. Muller.** 1993. Progress in scanning electron microscopy of frozen-hydrated biological specimens. Scanning Microsc. **7:**343–349.
24. **Hofemeister, H., and P. O'Hare.** 2008. Nuclear pore composition and gating in herpes simplex virus-infected cells. J. Virol. **82:**8392–8399.
25. **Kubitscheck, U., and R. Peters.** 1998. Localization of single nuclear pore complexes by confocal laser scanning microscopy and analysis of their distribution. Methods Cell Biol. **53:**79–98.
26. **Kubitscheck, U., P. Wedekind, O. Zeidler, M. Grote, and R. Peters.** 1996. Single nuclear pores visualized by confocal microscopy and image processing. Biophys. J. **70:**2067–2077.
27. **Leuzinger, H., U. Ziegler, C. Fraefel, E. M. Schraner, D. Glauser, I. Held, M. Ackermann, M. Müller, and P. Wild.** 2005. Herpes simplex virus 1 envelopment follows two diverse pathways. J. Virol. **79:**13047–13059.
28. **Lim, R. Y., and B. Fahrenkrog.** 2006. The nuclear pore complex up close. Curr. Opin. Cell Biol. **18:**342–347.
29. **Maul, G.** 1977. The nuclear and cytoplasmic pore complex. Structure, dynamics, distribution and evolution. Int. Rev. Cytol. Suppl. **6:**75–186.
30. **Maul, G., J. W. Price, and M. W. Lieberman.** 1971. Formation and distribution of nuclear pore complexes in interphase. J. Cell Biol. **51:**405–418.
31. **Mettenleiter, T. C.** 2004. Budding events in herpesvirus morphogenesis. Virus Res. **106:**167–180.
32. **Mettenleiter, T. C.** 2002. Herpesvirus assembly and egress. J. Virol. **76:**1537–1547.
33. **Mettenleiter, T. C., B. G. Klupp, and H. Granzow.** 2006. Herpesvirus assembly: a tale of two membranes. Curr. Opin. Microbiol. **9:**423–429.
34. **Monaghan, P., H. Cook, P. Hawes, J. Simpson, and F. Tomley.** 2003. High-pressure freezing in the study of animal pathogens. J. Microsc. **212:**62–70.
35. **Monier, K., J. C. Armas, S. Etteldorf, P. Ghazal, and K. F. Sullivan.** 2000. Annexation of the interchromosomal space during viral infection. Nat. Cell Biol. **2:**661–665.
36. **Pante, N., and U. Aebi.** 1993. The nuclear pore complex. J. Cell Biol. **122:** 977–984.
37. **Pante, N., R. Bastos, I. McMorrow, B. Burke, and U. Aebi.** 1994. Interactions and three-dimensional localization of a group of nuclear pore complex proteins. J. Cell Biol. **126:**603–617.
38. **Pante, N., and M. Kann.** 2002. Nuclear pore complex is able to transport macromolecules with diameters of about 39 nm. Mol. Biol. Cell **13:**425–434.
39. **Pante, N., F. Thomas, U. Aebi, B. Burke, and R. Bastos.** 2000. Recombinant Nup153 incorporates in vivo into Xenopus oocyte nuclear pore complexes. J. Struct. Biol. **129:**306–312.
40. **Park, R., and J. D. Baines.** 2005. Herpes simplex virus type 1 infection induces activation and recruitment of protein kinase C to the nuclear membrane and increased phosphorylation of lamin B. J. Virol. **80:**494–504.
41. **Radsak, K., M. Eickmann, T. Mockenhaupt, E. Bogner, H. Kern, A. Eis-Hubinger, and M. Reschke.** 1996. Retrieval of human cytomegalovirus glycoprotein B from the infected cell surface for virus envelopment. Arch. Virol. **141:**557–572.
42. **Ray, N., and L. W. Enquist.** 2004. Transcriptional response of a common permissive cell type to infection by two diverse alphaherpesviruses. J. Virol. **78:**3489–3501.
43. **Reynolds, A. E., E. G. Wills, R. J. Roller, B. J. Ryckman, and J. D. Baines.** 2002. Ultrastructural localization of the herpes simplex virus type 1 U_L31, U_L34, and U_S3 proteins suggests specific roles in primary envelopment and egress of nucleocapsids. J. Virol. **76:**8939–8952.
44. **Roizman, B.** 2001. Herpes simplex viruses and their replication, p. 2399–2460. *In* B. N. Fields, D. M. Knipe, and P. M. Howley (ed.), Fields virology, 4th ed., vol. 2. Lipincott-Raven Publishers, Philadelphia, PA.
45. **Schwartz, J., and B. Roizman.** 1969. Concerning the egress of herpes simplex virus from infected cells: electron and light microscope observations. Virology **38:**42–49.
46. **Schwartz, T. U.** 2005. Modularity within the architecture of the nuclear pore complex. Curr. Opin. Struct. Biol. **15:**221–226.
47. **Schwarz-Herion, K., B. Maco, U. Sauder, and B. Fahrenkrog.** 2007. Domain topology of the p62 complex within the 3-D architecture of the nuclear pore complex. J. Mol. Biol. **370:**796–806.
48. **Simpson-Holley, M., R. C. Colgrove, G. Nalepa, J. W. Harper, and D. M. Knipe.** 2005. Identification and functional evaluation of cellular and viral factors involved in the alteration of nuclear architecture during herpes simplex virus 1 infection. J. Virol. **79:**12840–12851.
49. **Skepper, J. N., A. Whiteley, H. Browne, and A. Minson.** 2001. Herpes simplex virus nucleocapsids mature to progeny virions by an envelopment→deenvelopment→reenvelopment pathway. J. Virol. **75:**5697–5702.
50. **Spring, S. B., B. Roizman, and J. Schwartz.** 1968. Herpes simplex virus products in productive and abortive infection. II. Electron microscopic and immunological evidence for failure of virus envelopment as a cause of abortive infection. J. Virol. **2:**384–392.
51. **Stannard, L. M., S. Himmelhoch, and S. Wynchank.** 1996. Intra-nuclear localization of two envelope proteins, gB and gD, of herpes simplex virus. Arch. Virol. **141:**505–524.
52. **Stoffler, D., B. Fahrenkrog, and U. Aebi.** 1999. The nuclear pore complex: from molecular architecture to functional dynamics. Curr. Opin. Cell Biol. **11:**391–401.
53. **Suntharalingam, M., and S. R. Wente.** 2003. Peering through the pore: nuclear pore complex structure, assembly, and function. Dev. Cell **4:**775–789.
54. **Torrisi, M. R., C. Di Lazzaro, A. Pavan, L. Pereira, and G. Campadelli-Fiume.** 1992. Herpes simplex virus envelopment and maturation studied by fracture label. J. Virol. **66:**554–561.
55. **Walther, P., Y. Chen, L. L. Pech, and J. B. Pawley.** 1992. High-resolution scanning electron microscopy of frozen-hydrated cells. J. Microsc. **168:**169–180.
56. **Walther, P., and M. Muller.** 1999. Biological ultrastructure as revealed by high resolution cryo-SEM of block faces after cryo-sectioning. J. Microsc. **196:**279–287.
57. **Walther, T. C., M. Fornerod, H. Pickersgill, M. Goldberg, T. D. Allen, and I. W. Mattaj.** 2001. The nucleoporin Nup153 is required for nuclear pore basket formation, nuclear pore complex anchoring and import of a subset of nuclear proteins. EMBO J. **20:**5703–5714.
58. **Whealy, M. E., J. P. Card, R. P. Meade, A. K. Robbins, and L. W. Enquist.** 1991. Effect of brefeldin A on alphaherpesvirus membrane protein glycosylation and virus egress. J. Virol. **65:**1066–1081.
59. **Wild, P., M. Engels, C. Senn, K. Tobler, U. Ziegler, E. M. Schraner, E. Loepfe, M. Ackermann, M. Mueller, and P. Walther.** 2005. Impairment of nuclear pores in bovine herpesvirus 1-infected MDBK cells. J. Virol. **79:** 1071–1083.
60. **Wild, P., E. M. Schraner, H. Adler, and B. M. Humbel.** 2001. Enhanced resolution of membranes in cultured cells by cryoimmobilization and freeze-substitution. Microsc. Res. Tech. **53:**313–321.
61. **Wild, P., E. M. Schraner, D. Cantieni, E. Loepfe, P. Walther, M. Mueller, and M. Engels.** 2002. The significance of the Golgi complex in envelopment of bovine herpesvirus 1 (BHV-1) as revealed by cryobased electron microscopy. Micron **33:**327–337.
62. **Yang, Q., M. P. Rout, and C. W. Akey.** 1998. Three-dimensional architecture of the isolated yeast nuclear pore complex: functional and evolutionary implications. Mol. Cell **1:**223–234.